Mon. Not. R. Astron. Soc. **000**, 000–000 (0000) Printed 26 April 2016 (MN LATEX style file v2.2)

Gas velocity patterns in simulated galaxies: Observational diagnostics of spiral structure theories

J. Baba[1,2⋆], K. Morokuma-Matsui[3,4], Y. Miyamoto[3], F. Egusa[4] and N. Kuno[3,5]
[1] *Earth-Life Science Institute, Tokyo Institute of Technology, 2-12-1 Ookayama, Meguro, Tokyo 152–8551, Japan.*
[2] *Research Center for Space and Cosmic Evolution, Ehime University, Bunkyo-cho 2-5, Matsuyama 790-8577, Japan*
[3] *Nobeyama Radio Observatory, National Astronomical Observatory of Japan, 462-2 Nobeyama, Minamimaki, Minamisaku, Nagano 384-1305, Japan*
[4] *Chile Observatory, National Astronomical Observatory of Japan, 2-21-1 Osawa, Mitaka, Tokyo 181–8588, Japan*
[5] *Division of Physics, Faculty of Pure and Applied Sciences, University of Tsukuba, Ten-noudai, Tsukuba, Ibaraki 305-8571, Japan*

arXiv:1604.06879v1 [astro-ph.GA] 23 Apr 2016

Accepted 2016 April 22. Received 2016 April 22; in original form 2016 February 12

ABSTRACT

There are two theories of stellar spiral arms in isolated disc galaxies that model stellar spiral arms with different longevities: quasi-stationary density wave theory, which characterises spirals as rigidly rotating, long-lived patterns (i.e. steady spirals), and dynamic spiral theory, which characterises spirals as differentially rotating, transient, recurrent patterns (i.e. dynamic spirals). In order to discriminate between these two spiral models observationally, we investigated the differences between the gas velocity patterns predicted by these two spiral models in hydrodynamic simulations. We found that the azimuthal phases of the velocity patterns relative to the gas density peaks (i.e. gaseous arms) differ between the two models, as do the gas flows; nevertheless, the velocity patterns themselves are similar for both models. Such similarity suggests that the mere existence of streaming motions does not conclusively confirm the steady spiral model. However, we found that the steady spiral model shows that the gaseous arms have *radial* streaming motions well inside the co-rotation radius, whereas the dynamic spiral model predicts that the gaseous arms tend to have *tangential* streaming motions. These differences suggest that the gas velocity patterns around spiral arms will enable distinction between the spiral theories.

Key words: galaxies: spiral — galaxies: kinematics and dynamics — galaxies: ISM — ISM: kinematic and dynamics — method: numerical

1 INTRODUCTION

Spiral structures are the most prominent features in disc galaxies. Near-infrared observations have shown that spiral structures are gravitationally driven variations in the surface densities of stellar discs (Block et al. 1994; Rix & Zaritsky 1995; Grosbøl et al. 2004; Elmegreen et al. 2011), which strongly suggests that spiral arms originate from the stellar dynamics in disc galaxies. Furthermore, observations of nearby spiral galaxies have shown that most of the star formation in spiral galaxies is associated with spiral arms (Lord & Young 1990; Cepa & Beckman 1990; Seigar & James 2002; Grosbøl & Dottori 2009). Accordingly, understanding how spiral arms in galaxies form and evolve is essential to understand both galactic dynamics and star formation, i.e. galaxy evolution. In this paper, we focus on spiral arms that arise in disc galaxies without external perturbations.

Major progress in theoretical studies on spiral structures was made in the 1960s–1980s by hypothesizing stellar spiral arms (hereafter, spiral arms) to be quasi-stationary density waves (Lindblad 1963; Lin & Shu 1964, 1966; Lin et al. 1969; Bertin et al. 1989a,b; Bertin & Lin 1996, for a review). In this so-called 'quasi-stationary spiral structure' (QSSS) hypothesis, spiral arms are supposed to be rigidly rotating, long-lived patterns (hereafter, 'steady spiral') that persist for at least several galactic rotations (i.e., $\gtrsim 1$ Gyr). Consequently, these steady spirals affect gas flows; when the gas inside a co-rotation radius ($R_{\rm CR}$) *overtakes* a spiral arm as it moves around a galactic disc, the gas is expected to form a standing shock, called a 'galactic shock', around the spiral arm (Fujimoto 1968; Roberts 1969; Shu et al. 1972, 1973; Sawa 1977; Ishibashi & Yoshii 1984; Lee & Shu 2012; Lee 2014) within one or two transits of the gas through the spiral arm ($\lesssim 100$ Myr; Woodward 1975; Roberts & Hausman 1984; Wada & Koda 2004; Wada 2008). The QSSS/galactic shock hypothesis predicts that the gas velocity changes suddenly; it is believed that such veloc-

⋆ E-mail:babajn@elsi.jp; baba@cosmos.phys.sci.ehime-u.ac.jp

ity changes are observed as wiggles in isovelocity contours of H_I/CO gas around the spiral arms of nearby galaxies such as M81 (e.g. Rots & Shane 1975; Rots 1975; Visser 1980) and M51 (e.g. Tully 1974; Rydbeck et al. 1985; Vogel et al. 1988; Rots et al. 1990; Garcia-Burillo et al. 1993; Kuno & Nakai 1997; Aalto et al. 1999; Miyamoto et al. 2014)[1]. Recent multi-dimensional hydrodynamic simulations have predicted that the shock (i.e. gaseous spiral arm) locations move *monotonically* from downstream to upstream of the stellar spiral arm with increasing radius (Gittins & Clarke 2004; Martínez-García et al. 2009; Kim & Kim 2014; Baba et al. 2015).

On the other hand, Goldreich & Lynden-Bell (1965) and Julian & Toomre (1966) proposed a transient spiral hypothesis based on linear local analyses of gaseous and stellar discs, respectively. Numerical simulations of galactic discs have extended this hypothesis to a transient recurrent spiral (hereafter, 'dynamic spiral') hypothesis (see a review by Dobbs & Baba 2014). According to this hypothesis, the amplitudes of spiral arms change on the timescale of a galactic rotation or even less (i.e. a few hundreds of Myrs) for multiple-arm spirals (Sellwood & Carlberg 1984; Fujii et al. 2011; Wada et al. 2011; Grand et al. 2012b; Baba et al. 2013; D'Onghia et al. 2013; Pettitt et al. 2015; Kumamoto & Noguchi 2016), unbarred grand-design spirals (Sellwood 2011)[2], and barred spirals (Baba et al. 2009; Grand et al. 2012a; Roca-Fàbrega et al. 2013; Baba 2015). In contrast to the QSSS/galactic shock hypothesis, the dynamic spiral model predicts that the gas does not flow through a spiral arm, but rather effectively falls into the spiral potential minimum from *both sides* of the arm (referred to as 'large-scale colliding flows'; Dobbs & Bonnell 2008; Wada et al. 2011). Furthermore, the dynamic spiral model shows *no systematic* offset between the gas density peak location and the spiral arm (Baba et al. 2015).

These recent advances in spiral theory require the determination of observational indicators that can be used to distinguish between steady and dynamic spirals. Some observational tests that could be employed for this purpose have been proposed (see a review by Dobbs & Baba 2014). It was proposed that the existence of radial metallicity distribution breaks could be used to test spiral longevity (Lépine et al. 2011; Scarano & Lépine 2013). On the other hand, focusing on the azimuthal direction, Dobbs & Pringle (2010) proposed that observations of the azimuthal distributions of age-dated stellar clusters could be used to discriminate among the spiral models (see also Wada et al. 2011; Grand et al. 2012a; Dobbs et al. 2014). The measurements of the azimuthal colour gradients across spiral arms over wide radial ranges could also be employed to test spiral longevity (Martínez-García & González-López lira 2013; Martínez-García & Puerari 2014). Furthermore, Baba et al. (2015) focused on spatial distributions of gas and old stars and suggested that radial profiles of the gas-star offset angles can be used to distinguish between the two spiral models. For the *kinematics* of gas and stars, Kawata et al. (2014) performed analyses using snapshots of N-body/hydrodynamic simulations of a Milky Way-sized barred spiral galaxy and predicted observational signatures of dynamic spirals (see also Baba et al. 2009). Recently, Grand et al. (2015) investigated the differences among the peculiar velocity power spectra of stars in the Milky Way galaxy predicted by the two spiral models and discussed a possible application to observations of gas velocity fields in external galaxies.

In this study, in order to develop a new method of distinguishing between the two spiral models, we focused on the differences between their gas velocity pattern predictions around spiral arms, because gas velocity data are more easily obtainable than measurements of stars in external galaxies. The remainder of this paper is organized as follows: In Section 2, we present the models and methods. Section 3 describes the differences between the gas velocity patterns predicted by the two spiral models. Section 4 summarizes our results and discusses an application of the results to observational data from spiral galaxies. We emphasize that this 'velocity pattern method' is not the only means of distinguishing between the spiral models. In order to determine the nature of spiral galaxies, other methods, such as CO-Hα offset measurement (Egusa et al. 2009) and gas-star offset measurement (Baba et al. 2015), are complementary to the velocity pattern method proposed in this paper.

2 NUMERICAL SIMULATIONS

2.1 Numerical methods

To investigate the differences between the gas velocity patterns around the spiral arms that are predicted by the steady and dynamic spiral models, we conducted hydrodynamic simulations of rigidly rotating spiral potentials (i.e. the steady spiral model; Section 2.3) and N-body/hydrodynamic simulations of stellar and gaseous discs (i.e. the dynamic spiral model; Section 2.2). These simulations were performed with an N-body/smoothed particle hydrodynamics (SPH) simulation code, `ASURA-2` (Saitoh & Makino 2009, 2010). The self-gravity was calculated with the Tree/GRavity PipE (GRAPE) method using a software emulator of GRAPE known as Phantom-GRAPE (Tanikawa et al. 2013).

[1] It is believed that the grand-design spirals of M51 and M81 are driven by tidal interactions with companion galaxies (e.g. Toomre 1981; Sundelius et al. 1987; Howard & Byrd 1990; Thomasson & Donner 1993; Salo & Laurikainen 2000a,b; Dobbs et al. 2010). See also Section 4.

[2] The longevity of (unbarred) grand-design spirals is a standing problem. Some early reports stated that numerical simulations had succeeded in reproducing unbarred long-lived grand-design spirals (Thomasson et al. 1990; Zhang 1996). However, Sellwood (2011) tested the same models and found that two-armed spirals are not single long-lived patterns, but rather the superpositions of three or more patterns that each grow and decay. More recently, Sellwood & Carlberg (2014) reported the existence of longer-lived modes, which survive multiple rotations (see also Roškar et al. 2012; Minchev et al. 2012). Nevertheless, Sellwood & Carlberg (2014) argued that their results were inconsistent with the idea that spiral arms are quasi-stationary density waves because the arms in their simulations changed with time. The origins of (unbarred) grand-design spirals are unclear, which are beyond of the scope of this study, although it is worth mentioning that tidal interactions could create and re-energize unbarred grand-design spirals (e.g. Byrd & Howard 1992; Oh et al. 2015; Pettitt et al. 2016).

The simulations also took into account radiative cooling and heating due to interstellar far-ultraviolet radiation (FUV; Wolfire et al. 1995). The radiative cooling of the gases was determined by assuming an optically thin cooling function, $\Lambda(T, f_{\rm H2}, G_0)$, based on a radiative transfer model of photo-dissociation regions across a wide temperature (T) range of 20 K $< T <$ 10^8 K (Wada et al. 2009). Here, the molecular hydrogen fraction, $f_{\rm H2}$, follows the fitting formula given by Gnedin & Kravtsov (2011), and G_0 is the FUV intensity normalized to the solar neighbourhood value. The normalized FUV intensity of an SPH particle is given by $G_0 = G_{0,\rm thin} e^{-\sigma_{1000} N_{\rm H}}$, where $N_{\rm H}$ is the total column density of hydrogen, $\sigma_{1000} = 2 \times 10^{-21}$ cm^2 is the effective cross-section for dust extinction at $\lambda = 1000$ Å (Draine & Bertoldi 1996; Glover & Mac Low 2007), and $G_{0,\rm thin}$ is the normalized FUV intensity in the optically-thin limit, which is given by summing over all stellar particles (Gerritsen & Icke 1997; Pelupessy et al. 2006). We determined the time-dependent FUV luminosities of the stellar particles by mapping their ages using the stellar population synthesis modelling software PEGASE (Fioc & Rocca-Volmerange 1997). $N_{\rm H}$ was computed using a Sobolev-like approximation (Gnedin et al. 2009).

We implemented sub-grid models for star formation and stellar feedback. Star formation was incorporated into the simulation as follows. If an SPH particle (with density n, temperature T, and velocity $\mathbf{v}$) satisfied the following criteria: (1) $n > 100$ cm^{-3}; (2) $T < 100$ K; and (3) $\nabla \cdot \mathbf{v} < 0$; then the SPH particle created star particles in a probabilistic manner following the Schmidt law, with a local dimensionless star formation efficiency of $C_* = 0.033$ (Saitoh et al. 2008). Feedback from type-II supernovae was implemented as thermal energy (Saitoh et al. 2008; Saitoh & Makino 2009), and H$_{\rm II}$-region feedback was considered using a Stromgren volume approach, in which the gases around young stars extending out to a radius that is sufficiently large to achieve ionization balance were simply defined as having a temperature of 10^4 K (Baba et al. 2016).

2.2 Dynamic spiral model

In order to investigate the velocity patterns in the dynamic spiral model, we used a 3D N-body/SPH simulation of a barred spiral galaxy (see Baba 2015, for details). In this model, the initial axisymmetric model is comprised of stellar and gaseous discs, a classical bulge, and a dark matter halo, which follow exponential, Hernquist (Hernquist 1990), and Navarro-Frenk-White (Navarro et al. 1997) profiles, respectively. The dark matter halo is treated as a fixed external potential. In this study, the initial numbers of stars and SPH particles were 6.4 and 4.5 million, respectively, and the gravitational softening length was 10 pc. Hereafter, we refer to this barred spiral galaxy model as the 'DYNAMIC' model.

The DYNAMIC model satisfies the criteria for bar instability (Efstathiou et al. 1982) and produces spontaneous stellar bar development. Baba (2015) found that the short-term behaviours of spiral arms in the outer regions ($R >$ 1.5–2 bar radii; i.e. $R \gtrsim 5$ kpc) can be explained by swing amplification theory (e.g. Toomre 1981); consequently, the effects of bars are not negligible in the inner regions ($R <$ 1.5–2 bar radii; i.e. $R \lesssim 5$ kpc). Thus, for the DYNAMIC model, we focus on the spiral arms regions with $R > 6$ kpc.

2.3 Steady spiral model

We performed hydrodynamic simulations in a static axisymmetric potential, $\Phi_0(R, z)$, with a rigidly rotating spiral potential, $\Phi_{\rm sp}(R, \phi, z; t)$. Hereafter, we refer to this model as the 'STEADY' model. The static axisymmetric potential was produced by using the cloud-in-cell (CIC) mass-assignment scheme from the initial condition of the DYNAMIC model. The initial conditions for the gaseous disc were identical to those of the DYNAMIC model. The initial number of SPH particles and the gravitational softening length were the same as those in the DYNAMIC model.

The gravitational potential of the spiral arm[3] was calculated using

$$\Phi_{\rm sp}(R, \phi, z; t) = A(R, z) \frac{z_0}{\sqrt{z^2 + z_0^2}} \times \cos\left[m \left\{ \phi - \Omega_{\rm p} t + \cot i_{\rm sp} \left(\ln \frac{R}{R_0} \right) \right\} \right], \quad (1)$$

where A, m, $i_{\rm sp}$, $\Omega_{\rm p}$, and z_0 are the amplitude of the spiral potential, the number of stellar spiral arms, the pitch angle, the pattern speed, and the scale height, respectively. In this study, we used $z_0 = 100$ pc and $R_0 = 1$ kpc. The spiral potential amplitude was controlled by the following dimensionless parameter:

$$\mathcal{F} \equiv \frac{m|A|}{|\Phi_0| \sin i_{\rm sp}}, \quad (2)$$

which represents the gravitational force due to the spiral arms in the direction perpendicular to the arms relative to the radial force from the background axisymmetric potential (Shu et al. 1973). To model typical two-armed (i.e. $m = 2$) spiral galaxies, we used a typical $i_{\rm sp}$ of 25°, which was determined based on observations of external spiral galaxies (e.g. Grosbøl et al. 2004). Since a gravitational potential is not a directly observed value, we used $\mathcal{F} = 5\%$ because of the results of theoretical studies of self-consistent steady spiral models (e.g. Grosbol 1993)[4]. Although the value of $\Omega_{\rm p}$ is arbitrary and varies among galaxies, the aforementioned self-consistent steady spiral models suggest that a steady spiral can extend up to or beyond its CR radius. To analyse the gas velocity patterns at the same radii as those in DYNAMIC model (i.e. $R > 6$ kpc; see Section 2.2), we thus used

[3] In the present study, we adopted a simple cosine function for the spiral potential, which is shown in eq.(1). Nevertheless, as argued by Kalnajs (1973), the potential perturbations from (stellar) spiral arms should result from the crowding of 'stellar' orbits in a galactic disc. In fact, more detailed studies of self-consistent steady spiral models have shown that self-consistent spiral potentials are not described by simple cosine functions in the azimuthal direction (e.g. Pichardo et al. 2003; Junqueira et al. 2013). However, whether the spiral potential is modeled as cosine or Gaussian does not affect our objectives, since the both spiral-potential models are symmetric with respect to the spiral.

[4] According to studies of self-consistent steady spiral models, the effects of nonlinear stellar dynamics cause self-consistent spirals to terminate at the 4/1 resonance and would damp self-consistent spirals for $\mathcal{F} \gtrsim 5\%$ (Contopoulos & Grosbol 1988; Patsis et al. 1991).

$R_{\rm CR} \simeq 15$ kpc, which corresponds $\Omega_{\rm p} \simeq 16$ km s^{-1} kpc^{-1} in the STEADY model.

3 GAS FLOWS AND VELOCITY PATTERNS AROUND SPIRAL ARMS

We present spatial distributions of the gas density and velocity around spiral arms in the STEADY and DYNAMIC models. In Section 3.1, we examine the differences between the spatial distributions and gas flows in the two spiral models. These results support those presented in Baba et al. (2015). Next we present the similarities and differences between the velocity patterns of the gas in the STEADY and DYNAMIC spiral models in Sections 3.2 and 3.3, respectively.

3.1 Spatial distributions and flows of gas

Fig. 1 shows the surface density distributions of H_2 gas in the STEADY model. Molecular gas forms the main two-arm spirals along the (stellar) spiral arms. There are also many substructures, i.e. 'feathers' or 'spurs', between the spirals and on the downstream sides of the spirals, as observed in actual spiral galaxies (e.g. Elmegreen 1980; La Vigne et al. 2006). Because $R_{\rm CR} = 15$ kpc, the gas shown in these panels overtakes the spiral arms. For purpose of demonstration, the trajectories of two SPH particles are plotted (as red lines with symbols) in the left panel; as shown, the SPH particles flow into the spiral from the trailing side, and experience a sudden change in direction due to galactic shocks, and then pass through the spiral onto the leading side.

The situation differs in the DYNAMIC model, for which the the surface density distributions of the molecular gas are shown in Fig. 2. The molecular spiral arms are clear at $t = 2.776$ Gyr, but are weak at the other times. Such time evolution originates from the evolution of the stellar spirals. As shown Fig. 3, the amplitudes ($|B_{m=2}|$), rotational frequencies ($\Omega_{\rm phase}$), and pitch angles ($i_{\rm sp}$) of the spiral arms are not constant, but change within ~ 100 Myr (i.e. $\lesssim$ the typical rotational period of a galaxy). In other words, the grand-design (stellar) spiral arms in the DYNAMIC model are not stationary, but rather transient recurrent (i.e. dynamic; Baba 2015). To compare the gas flow with that in the STEADY model, the SPH particle trajectories were overlaid on the gas density maps, as shown in Fig. 2. In contrast to the STEADY model, in the DYNAMIC model, the SPH particle trajectories that are overlaid on the x-y map of the gas show that gas and stars fall into the spiral arm from both sides, rather than from just one side (see also Dobbs & Bonnell 2008; Wada et al. 2011; Kawata et al. 2014)[5].

The left panels of Fig. 4 show that, in the STEADY model, the primary gas density peaks (i.e. gaseous spiral arms) occur on the downstream sides of the spiral potential minima at all presented radii (see also the right panel of Fig. 1)[6]. Such radial dependence of the positions of the gaseous arms relative to spiral arms has been indicated by previous hydrodynamic simulations of steady spiral models (e.g. Gittins & Clarke 2004; Baba et al. 2015). In contrast, the DYNAMIC model (right panels of Fig. 4) shows no systematic offset between the gaseous and spiral arms. The same results have been reported in previous studies (e.g. Baba et al. 2015).

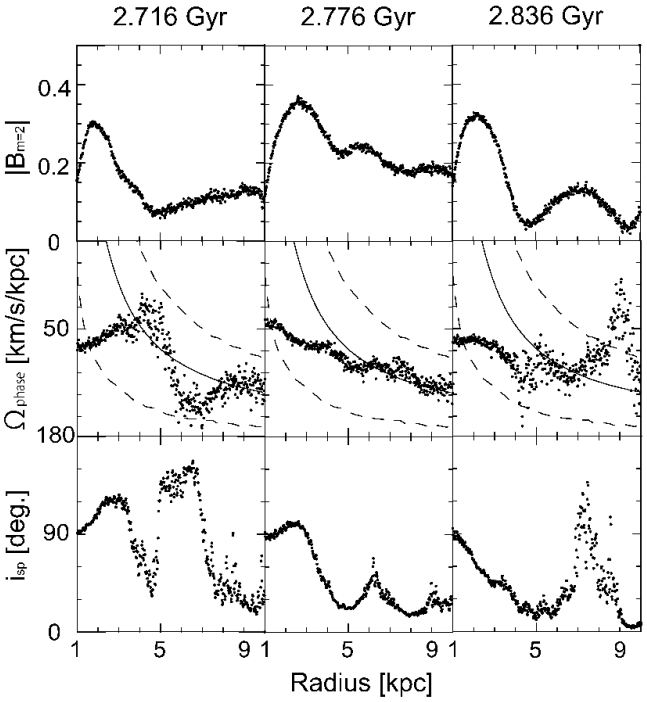

Figure 3. Radial profiles of the grand-design spiral arm parameters ($m = 2$) in DYNAMIC model at times corresponding to snapshots shown in Fig. 2. Top: spiral amplitude $|B_{m=2}|$. Middle: angular phase speed $\Omega_{\rm phase}$ [km s^{-1} kpc^{-1}]. Solid and dashed curves indicate circular rotational frequency $\Omega_{\rm cir}$ and $\Omega_{\rm cir} \pm \kappa/2$ (here, κ is epicyclic frequency), respectively. Bottom: pitch angle $i_{\rm sp}$ [degrees]. These spiral parameters were analysed using 1D Fourier decomposition of stellar surface density distributions with respect to azimuthal direction at each radius (See Section 2.3 of Baba 2015).

3.2 Streaming motions in steady spiral model

The azimuthal profiles of the gas velocities in the STEADY model are shown in the left panels of Fig. 4. The vertical blue shaded regions indicate the positions of the gaseous spiral arms. Focusing on the streaming motions of the gaseous spiral arms, it is evident that the gaseous spiral arms are

[5] In this paper, we focus on gas motions, but similar behaviour of stars has been observed for stars in previous simulation results (Sellwood & Binney 2002; Grand et al. 2012b,a; Roškar et al. 2012; Baba et al. 2013; Grand et al. 2014; Kawata et al. 2014).

[6] The secondary gas density peaks also occur downstream from the primary peaks, e.g. $\phi \simeq 260°$, $200°$, and $190°$ at $R = 6.0$, 7.0, and 8.0 kpc, respectively, and correspond to the spurs (see the right panel of Fig. 1). The existence of such secondary peaks was previously observed in early galactic shock calculations (e.g. Roberts 1969; Shu et al. 1973), although the origins of the secondary peaks are beyond the scope of this paper. See Dobbs & Baba (2014) and the references therein for discussions of their origins.

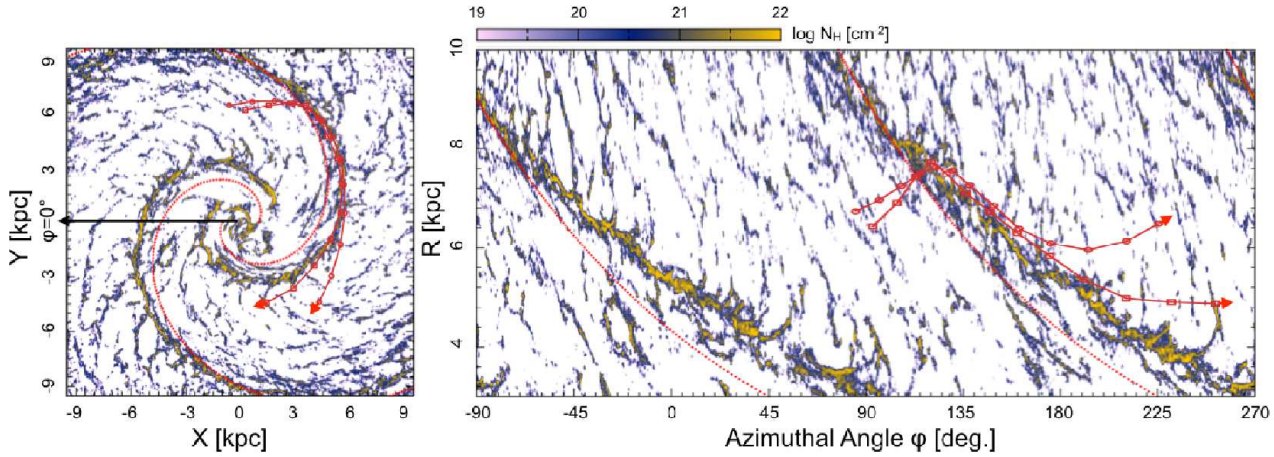

Figure 1. Spatial distributions of molecular gas in the $x-y$ plane (left) and the $R-\phi$ plane (right) in the STEADY model at $t = 360$ Myr. Solid lines with symbols indicate SPH particle trajectories. Dotted red lines indicate minima of of spiral potential. Time evolutions are shown in a rotating frame of the spiral arm.

associated with the V_R minima and $V_\phi \simeq \bar{V}_\phi$, where $\bar{V}_\phi$ is the average rotational velocity, i.e. the galactic rotational velocity. Such streaming patterns do not depend on the pitch angle of the steady spiral within the range of observed pitch angles $10^\circ \lesssim i_{\rm sp} \lesssim 40^\circ$ (e.g. Grosbøl et al. 2004). Therefore, it is suggested that if an observed spiral galaxy has steady stellar spiral arms, the gas in the *gaseous* spiral arms is expected to exhibit strong *radial* streaming motions and weak tangential streaming motions, at least well inside $R_{\rm CR}$.

This result is consistent with the predictions of the linear density wave theory (Lin et al. 1969; Burton 1971) and the QSSS/galactic shock hypothesis (i.e. non-linear density wave theory; cf. Fig. 5 of Roberts 1969). More specifically, the QSSS/galactic shock hypothesis predicts that V_R steeply decreases toward the location of maximum gas compression (i.e. the gaseous spiral arm), reaches its minimum, and then increases on the outer side of the arm. Furthermore, this theory predicts that V_ϕ decrease just before the gas enters the stellar spiral arm, and then increases steeply in the arm. Therefore, gaseous arms are located to be at a transition points from a V_ϕ minima to a V_ϕ maxima.

In contrast to the patterns in gaseous arms, the gas streaming in the *stellar* spirals are radius-dependent. From the left panels of Fig. 4, it is evident that when $R = 6.0$ kpc, the gases in the stellar spirals (represented by vertical dashed lines) have $V_R \simeq 0$ as well as V_ϕ minima, whereas when $R = 8.0$ kpc they have the V_R-minima and $V_\phi \simeq \bar{V}_\phi$. These differences result from the radial dependences of the positions of gaseous arms (vertical blue shaded regions) relative to stellar spirals (vertical dashed lines).

3.3 Streaming motions in dynamic spiral model

The right panels of Fig. 4 show the azimuthal gas velocity profiles in the DYNAMIC model. Although the gas flows with respect to the spiral arms in the DYNAMIC model are completely different from those in the STEADY model (see Section 3.1), the velocity profiles of the two models are similar. This similarity is due to the convergence of gas from both side of a spiral arm. The gas whose guiding centre is at an inner (outer) radius enters a spiral arm from behind (in front of) the arm, and then form a clear grand-design spiral at $t \simeq 2.776$ Gyr (right panels of Fig. 3). These directions of the motions are due to epicyclic motion[7], whose directions are opposite to the galactic rotation direction. In other words, in order to conserve angular momentum, V_ϕ must be larger when the star or gas is closer to the galactic centre than when it is farther away. In this case, the gas behind (in front of) a spiral arm tends to have velocities of $V_R < 0$ ($V_R > 0$) and $V_\phi \gtrsim \bar{V}_\phi$ ($V_\phi \lesssim \bar{V}_\phi$).

Although the overall velocity patterns in the DYNAMIC model are similar to those of the STEADY model, the details differ. Focusing on the streaming motions of the *gaseous* arms in the DYNAMIC model, it is evident that the V_R minima are not associated with the gaseous arms; instead, the gaseous arms have velocities of $V_R \simeq 0$ and $\bar{V}_\phi \lesssim V_\phi \lesssim V_{\phi,\rm max}$ (right panels of Fig. 4). These velocity patterns result from the fact that stellar spiral arms are formed by flows from both sides of the arms, and that gas is associated with this accumulation process (see below).

In order to explain why these velocity patterns occur in the dynamic spiral model, we consider a simple model in which a galaxy has a flat rotation curve at velocity $V_{\rm cir}$ and a spiral arm is formed by the collision between epicyclic flows with guiding centres at an inner radius ($R_{\rm in}$) and an outer radius ($R_{\rm out}$). The masses of the flows from the inner and outer radii are assumed to be $M_{\rm in}$ and $M_{\rm out}$, respectively. A schematic of this simple model is presented in Fig. 5. Assuming angular momentum conservation, the angular momentum of the arm is given by $L_{\rm arm} = M_{\rm in}R_{\rm in}V_{\rm cir} + M_{\rm out}R_{\rm out}V_{\rm cir}$, and the mass of the arm is $M_{\rm arm} = M_{\rm in} + M_{\rm out}$. Thus, the rotational velocity of the

[7] In general, the phrase 'epicyclic motion' refers to near-circular motion (Binney & Tremaine 2008). However, in this paper, we also use this phrase to describe non-circular orbits with finite radial amplitudes.

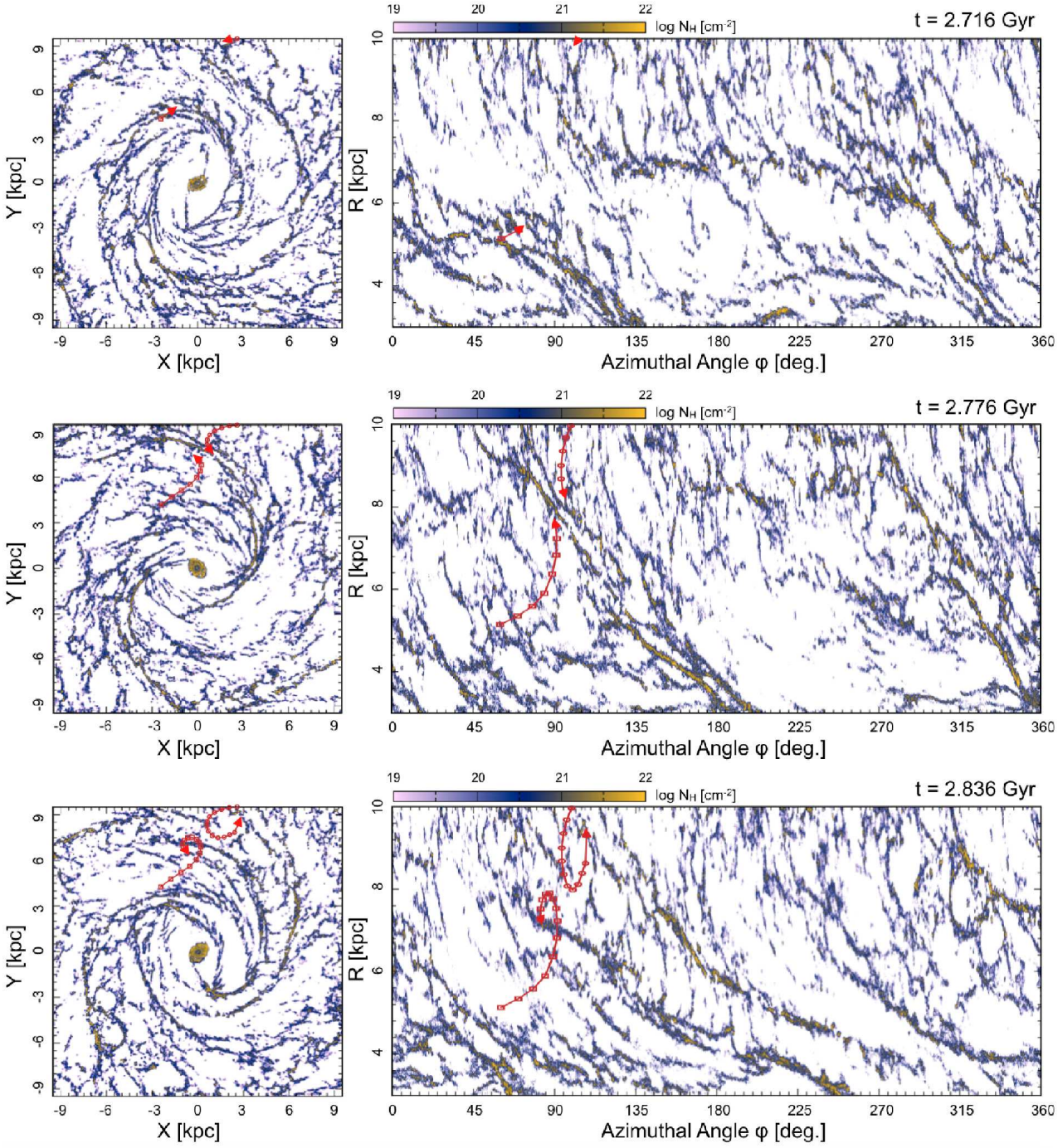

Figure 2. Same as Fig. 1, but for DYNAMIC model at $t = 2.716$ Gyr, 2.776 Gyr, and 2.836 Gyr, from top to bottom. Red lines with symbols in the $x-y$ plane indicate SPH particle trajectories. Time evolution is shown in frame rotating at $\Omega = 25$ km s^{-1} kpc^{-1}, which corresponds to galactic rotational angular frequency at $R \simeq 8$ kpc. Note that in the inner part of the disc ($R \lesssim 3$ kpc) the simulated galaxy shows also the characteristic features, such as offset ridges and inner rings, which are formed by the stella bars (e.g. Athanassoula 1992; Byrd et al. 2006).

arm ($V_{\rm arm}$) formed at $R_{\rm arm}$ is given by

$$V_{\rm arm} = \frac{L_{\rm arm}}{M_{\rm arm} R_{\rm arm}} = \frac{M_{\rm in} R_{\rm in} + M_{\rm out} R_{\rm out}}{(M_{\rm in} + M_{\rm out}) R_{\rm arm}} V_{\rm cir} = \frac{R_{\rm m}}{R_{\rm arm}} V_{\rm cir}, \quad (3)$$

where $R_{\rm m} \equiv (M_{\rm in} R_{\rm in} + M_{\rm out} R_{\rm out})/(M_{\rm in} + M_{\rm out})$ is the mass-weighted average radius of the raw material forming the arm, and can be rewritten as follows

$$R_{\rm m} = \frac{M_{\rm out}(R_{\rm out} - R_{\rm arm}) - M_{\rm in}(R_{\rm arm} - R_{\rm in})}{M_{\rm in} + M_{\rm out}} + R_{\rm arm}. \quad (4)$$

To calculate $R_{\rm m}$, we first consider the simple case of

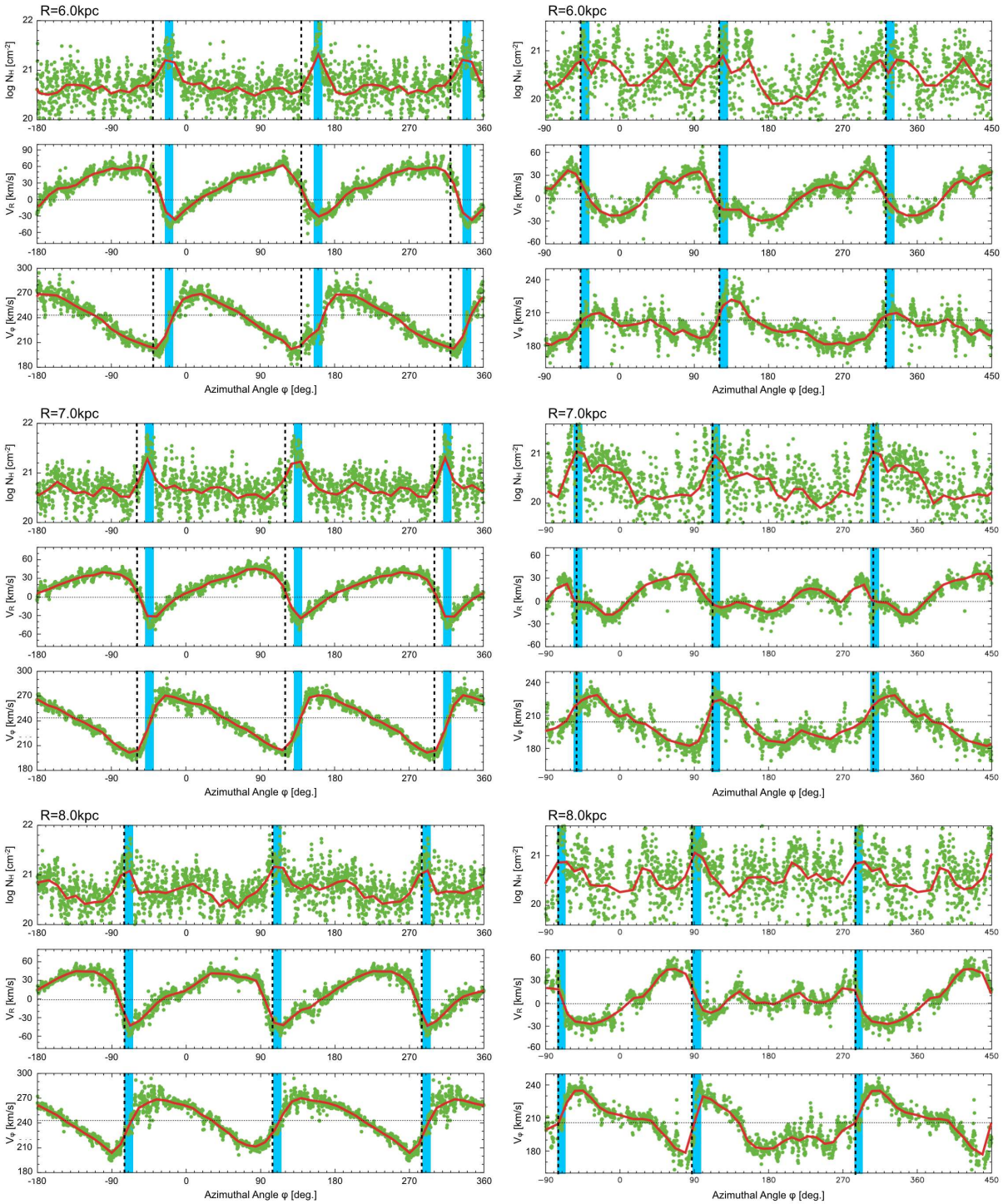

Figure 4. Left: Azimuthal profiles of $N_{\rm H}$ (top), V_R (middle) and V_ϕ (bottom) of gas in STEADY model (shown in Fig. 1) at $R = 6.0$ kpc, 7.0 kpc, and 8.0 kpc. Gas flows from left ($\phi < 0$) to right ($\phi > 0$) for the STEADY model. Solid curves fit averaged values over 5 Myr using a cubic spline interpolation. Horizontal dotted lines indicate average velocities at each radius, respectively. Vertical black dashed lines and vertical blue shaded regions indicate positions of spiral potential minimum and gas density maximum, respectively. Right: Same as left panels, but for DYNAMIC model (shown in Fig. 2) at $R = 6.0$ kpc, 7.0 kpc, and 8.0 kpc. Time is $t = 2.776$ Gyr.

$M_{\rm in} = M_{\rm out}$. In this case,

$$R_{\rm m} = \frac{(R_{\rm out} - R_{\rm arm}) - (R_{\rm arm} - R_{\rm in})}{2} + R_{\rm arm}. \quad (5)$$

Typically, the epicyclic amplitude is approximated by the wavelength at the minimum frequency of the Lin–Shu–Kalnajs dispersion relation $\lambda_{\rm min} = \lambda_{\rm crit} Q$, where $\lambda_{\rm crit}$ is Toomre's critical wavelength and Q is the Toomre's Q parameter[8]. Thus,

$$R_{\rm out} - R_{\rm arm} \approx \lambda_{\rm min}(R_{\rm out}) \quad (6)$$

and

$$R_{\rm arm} - R_{\rm in} \approx \lambda_{\rm min}(R_{\rm in}). \quad (7)$$

Since dynamic spiral arms develop from a structure with a wavelength of $\lambda_{\rm crit}$ via the swing amplification mechanism (e.g. Carlberg & Freedman 1985; Fujii et al. 2011; Baba et al. 2013), $\lambda_{\rm crit}$ can be approximated as follows

$$\lambda_{\rm crit}(R) = \frac{2\pi R}{m X_{\rm GT}} \approx 2R, \quad (8)$$

where m is the number of arms, and $X_{\rm GT}$ is Goldreich & Tremaine's parameter (see equation (19) of Dobbs & Baba 2014); $m = 2$ and $X_{\rm GT} \approx 1.5$ for maximum amplification (see Fig. 5 of Dobbs & Baba 2014, and see also Michikoshi & Kokubo (2016)). Thus, if $Q(R_{\rm out}) \approx Q(R_{\rm in}) \approx 1$,

$$R_{\rm m} \approx \frac{\lambda_{\rm min}(R_{\rm out}) - \lambda_{\rm min}(R_{\rm in})}{2} + R_{\rm arm} \approx (R_{\rm out} - R_{\rm in}) + R_{\rm arm} > R_{\rm arm}. \quad (9)$$

That is $R_{\rm m}/R_{\rm arm} > 1$, resulting in $V_{\rm arm} > V_{\rm cir}$ from equation (3).

However, $M_{\rm in}$ might be larger than $M_{\rm out}$ because the radial mass distributions in disc galaxies tend to follow exponential profiles. In such cases, the difference between $M_{\rm in}(R_{\rm arm} - R_{\rm in})$ and $M_{\rm out}(R_{\rm out} - R_{\rm arm})$ tends to decrease, resulting in the condition $V_{\rm arm} \simeq V_{\rm cir}$. It is therefore suggested that if an observed spiral galaxy has a dynamic spiral, then the *gaseous* arms should exhibit streaming motions with $V_{\rm arm} \gtrsim V_{\rm cir} \gtrsim \bar{V}_\phi$.

Finally, we discuss the gas streaming motions in the stellar spirals. Unlike in the STEADY model, in the DYNAMIC model, the gas streaming motions are nearly zero in the *stellar* arms regardless of the radius, because of the small offsets between gaseous arms and stellar arms.

4 SUMMARY AND IMPLICATIONS

In this paper, we analysed the results of hydrodynamic simulations and discussed the differences between the velocity patterns predicted by the steady and dynamic spiral models. The main results can be summarized as follows. The steady spiral model shows that

[8] Considering a disc with the radial velocity dispersion (σ_R) and epicyclic frequency (κ), a typical epicyclic amplitude ΔR is approximated by σ_R/κ (e.g. Bertin 2000). On the other hand, $\lambda_{\rm min} = \lambda_{\rm crit} Q = 4\sigma_R/\kappa$ (see equation (8) and Fig. 2 of Dobbs & Baba 2014). Thus, $\Delta R \sim \lambda_{\rm min}$.

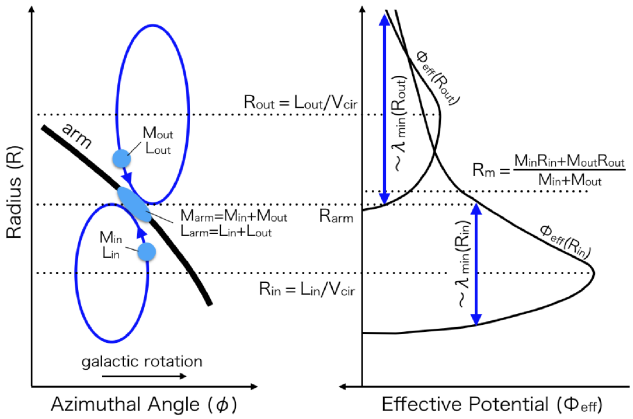

Figure 5. Schematic of dynamic spiral model, where spiral arm is formed by collision between epicyclic flows with guiding centres at $R_{\rm in}$ and $R_{\rm out}$. Details are described in Section 3.3.

(i) the locations of gaseous spiral arms move monotonically from downstream to upstream of the stellar spiral arms with increasing radius (see also Baba et al. 2015);

(ii) gaseous arms well inside the $R_{\rm CR}$ are associated with V_R minima and weak tangential streaming motions, i.e. *radial* streaming motions;

(iii) gas streaming patterns in the stellar spiral arms are radius-dependent, because of the radial dependence of the gaseous arms position relative to the stellar arm positions.

These results are consistent with the predictions of conventional galactic shock theory (Roberts 1969; Lin et al. 1969; Burton 1971). However, at least in terms of our simulations, the dynamic spiral simulation results suggest that

(i) no systematic offset exists between the gaseous arm and the stellar arms (see also Baba et al. 2015);

(ii) gaseous arms tend to associate with $V_R \simeq 0$ and $V_\phi \gtrsim \bar{V}_\phi$, i.e. *tangential* streaming motions;

(iii) gas streaming motions are nearly zero in the stellar spiral arms.

These results were obtained in the hydrodynamic simulations of isolated galaxy models, although we expect the velocity patterns of tidally induced spirals (e.g. M51 and M81) to differ between the steady and dynamic spiral models. According to N-body/hydrodynamic simulations (Dobbs et al. 2010) and N-body simulations (Oh et al. 2008, 2015) of tidally interacting systems, tidally-induced spirals are not quasi-stationary density waves, but *kinematic* density waves. Furthermore, these simulations suggested that the pattern speeds of tidally induced spirals clearly differ from the galactic angular speed, but decrease as the radius increases (Pettitt et al. 2016). This scenario illustrates intermediate behavior between the steady and dynamic spiral models. In this case, the gas enters into a spiral arm from one side of the arm, and then experiences a sudden compression such as a galactic shock. Thus, it is expected that the gaseous spiral arms in tidally induced spiral galaxies also have radial streaming motions, which is is consistent with previous observations of M51 (e.g. Kuno & Nakai 1997; Shetty et al. 2007; Miyamoto et al. 2014). However, in contrast to the steady spiral model (see Section 3.2), the gas streaming ve-

locities in *stellar* arms might not vary with radius, because the positions of the gaseous arms relative to the tidally induced stellar spirals are not expected to be strongly radius-dependent.

These differences encourage the use of gas velocity patterns in spiral galaxies for observational spiral model tests. Our simulations showed that the streaming velocity is typically ~ 10 km s^{-1} and that the offset between stellar and gaseous arms is typically $\lesssim 1$ kpc, suggesting that the required spatial and velocity resolutions are at least $\lesssim 1$ kpc and ~ 10 km s^{-1}, respectively. In addition, this 'velocity pattern method' requires gas detection in both the arm and inter-arm regions. These spatial and velocity resolutions are easily achievable with existing instruments, although the gas detection sensitivity in inter-arm regions is somewhat problematic (except for nearest galaxies). It is therefore useful to conduct high-sensitivity observations of the arm and inter-arm region with the latest generation of instruments such as the Atacama Large Millimeter/submillimeter Array (ALMA) and the Square Kilometre Array (SKA).

Nevertheless, an accurate method of determining gas velocity patterns in galaxies requires further study, because it is only possible to measure the line-of-sight velocity of a gas. In other words, one cannot directly measure both V_R and V_ϕ at the same point in a galaxy. In fact, the conventional streaming velocity measurement method is based on analysing the position-velocity (PV) diagrams along the major and minor axes of the observed spiral galaxies (e.g. Aalto et al. 1999); tangential streaming should be most apparent along the major axis, whereas radial streaming should be most apparent along the minor axis. However, the PV diagram method can be used to determine *local* streaming motions only at the points at which the spiral arm lies across the major or minor axis. In short, the PV diagram method cannot be used to ascertain the *global* distributions of streaming motions in observed spiral galaxies. Thus, in order to determine these global distributions of streaming motions, the 2D gas velocity fields in spiral galaxies must be acquired using another method, such as that proposed proposed by Kuno & Nakai (1997) (see also Fig. 10 of Miyamoto et al. 2014). Methods of modelling spiral galaxy 2D velocity fields based on observational data will be useful to discriminate between the spiral models and will be presented in future reports.

Finally, we note that the velocity patterns themselves are similar between the two spiral models and suggest that such similarity indicates that the kinematic method should not be used to determine $R_{\rm CR}$ from residual velocity fields or streaming motion direction changes. In fact, if one applies this so-called 'geometric phase method' (Canzian 1993) to determine $R_{\rm CR}$ (or a pattern speed) for a spiral galaxy with *dynamic* spirals, an $R_{\rm CR}$ value greater than the disc radius will be obtained. Furthermore, the similarity between the two spiral models suggests that the existence of streaming motions is not conclusive evidence of the steady spiral model (i.e. the QSSS/galactic shock hypothesis). Therefore, it is important to analyse the global gas velocity patterns, along with CO-Hα offset measurements (Egusa et al. 2009) and gas-star offset measurements (Baba et al. 2015) to distinguish the spiral models.

ACKNOWLEDGEMENTS

We would like to thank the referees for their critical comments and informative reports which improved this paper. We thank Takayuki R. Saitoh, Michiko S. Fujii and Keiichi Wada for a careful reading of the manuscript and constructive comments. Calculations, numerical analyses and visualization were carried out on Cray XC30, and computers at Center for Computational Astrophysics, National Astronomical Observatory of Japan. This research was supported by HPCI Strategic Program Field 5 'The origin of matter and the universe' and JSPS Grant-in-Aid for Young Scientists (B) Grant Number 26800099.

REFERENCES

Aalto, S., Hüttemeister, S., Scoville, N. Z., & Thaddeus, P. 1999, ApJ, 522, 165
Athanassoula, E. 1992, MNRAS, 259, 345
Baba, J. 2015, MNRAS, 454, 2954
Baba, J., Asaki, Y., Makino, J., Miyoshi, M., Saitoh, T. R., & Wada, K. 2009, ApJ, 706, 471
Baba, J., Morokuma-Matsui, K., & Egusa, F. 2015, PASJ, 67, L4
Baba, J., Morokuma-Matsui, K., & Saitoh, T. R. 2016, submitted
Baba, J., Saitoh, T. R., & Wada, K. 2013, ApJ, 763, 46
Bertin, G. 2000, Dynamics of Galaxies
Bertin, G., & Lin, C. C. 1996, Spiral structure in galaxies a density wave theory, ed. G. Bertin & C. C. Lin
Bertin, G., Lin, C. C., Lowe, S. A., & Thurstans, R. P. 1989a, ApJ, 338, 78
—. 1989b, ApJ, 338, 104
Binney, J., & Tremaine, S. 2008, Galactic Dynamics: Second Edition (Princeton University Press)
Block, D. L., Bertin, G., Stockton, A., Grosbol, P., Moorwood, A. F. M., & Peletier, R. F. 1994, A&A, 288, 365
Burton, W. B. 1971, A&A, 10, 76
Byrd, G. G., Freeman, T., & Buta, R. J. 2006, AJ, 131, 1377
Byrd, G. G., & Howard, S. 1992, AJ, 103, 1089
Canzian, B. 1993, ApJ, 414, 487
Carlberg, R. G., & Freedman, W. L. 1985, ApJ, 298, 486
Cepa, J., & Beckman, J. E. 1990, ApJ, 349, 497
Contopoulos, G., & Grosbol, P. 1988, A&A, 197, 83
Dobbs, C., & Baba, J. 2014, PASA, 31, 35
Dobbs, C. L., & Bonnell, I. A. 2008, MNRAS, 385, 1893
Dobbs, C. L., & Pringle, J. E. 2010, MNRAS, 409, 396
Dobbs, C. L., Pringle, J. E., & Naylor, T. 2014, MNRAS, 437, L31
Dobbs, C. L., Theis, C., Pringle, J. E., & Bate, M. R. 2010, MNRAS, 403, 625
D'Onghia, E., Vogelsberger, M., & Hernquist, L. 2013, ApJ, 766, 34
Draine, B. T., & Bertoldi, F. 1996, ApJ, 468, 269
Efstathiou, G., Lake, G., & Negroponte, J. 1982, MNRAS, 199, 1069
Egusa, F., Kohno, K., Sofue, Y., Nakanishi, H., & Komugi, S. 2009, ApJ, 697, 1870
Elmegreen, D. M. 1980, ApJ, 242, 528
Elmegreen, D. M. et al. 2011, ApJ, 737, 32

Fioc, M., & Rocca-Volmerange, B. 1997, A&A, 326, 950
Fujii, M. S., Baba, J., Saitoh, T. R., Makino, J., Kokubo, E., & Wada, K. 2011, ApJ, 730, 109
Fujimoto, M. 1968, in IAU Symposium, Vol. 29, IAU Symposium, 453
Garcia-Burillo, S., Combes, F., & Gerin, M. 1993, A&A, 274, 148
Gerritsen, J. P. E., & Icke, V. 1997, A&A, 325, 972
Gittins, D. M., & Clarke, C. J. 2004, MNRAS, 349, 909
Glover, S. C. O., & Mac Low, M.-M. 2007, ApJS, 169, 239
Gnedin, N. Y., & Kravtsov, A. V. 2011, ApJ, 728, 88
Gnedin, N. Y., Tassis, K., & Kravtsov, A. V. 2009, ApJ, 697, 55
Goldreich, P., & Lynden-Bell, D. 1965, MNRAS, 130, 125
Grand, R. J. J., Bovy, J., Kawata, D., Hunt, J. A. S., Famaey, B., Siebert, A., Monari, G., & Cropper, M. 2015, MNRAS, 453, 1867
Grand, R. J. J., Kawata, D., & Cropper, M. 2012a, MNRAS, 426, 167
—. 2012b, MNRAS, 421, 1529
—. 2014, MNRAS, 439, 623
Grosbol, P. 1993, PASP, 105, 651
Grosbøl, P., & Dottori, H. 2009, A&A, 499, L21
Grosbøl, P., Patsis, P. A., & Pompei, E. 2004, A&A, 423, 849
Hernquist, L. 1990, ApJ, 356, 359
Howard, S., & Byrd, G. G. 1990, AJ, 99, 1798
Ishibashi, S., & Yoshii, Y. 1984, PASJ, 36, 41
Julian, W. H., & Toomre, A. 1966, ApJ, 146, 810
Junqueira, T. C., Lépine, J. R. D., Braga, C. A. S., & Barros, D. A. 2013, A&A, 550, A91
Kalnajs, A. J. 1973, Proceedings of the Astronomical Society of Australia, 2, 174
Kawata, D., Hunt, J. A. S., Grand, R. J. J., Pasetto, S., & Cropper, M. 2014, MNRAS, 443, 2757
Kim, Y., & Kim, W.-T. 2014, MNRAS, 440, 208
Kumamoto, J., & Noguchi, M. 2016, arXiv160308761
Kuno, N., & Nakai, N. 1997, PASJ, 49, 279
La Vigne, M. A., Vogel, S. N., & Ostriker, E. C. 2006, ApJ, 650, 818
Lee, W.-K. 2014, ApJ, 792, 122
Lee, W.-K., & Shu, F. H. 2012, ApJ, 756, 45
Lépine, J. R. D. et al. 2011, MNRAS, 417, 698
Lin, C. C., & Shu, F. H. 1964, ApJ, 140, 646
—. 1966, Proceedings of the National Academy of Science, 55, 229
Lin, C. C., Yuan, C., & Shu, F. H. 1969, ApJ, 155, 721
Lindblad, B. 1963, Stockholms Observatoriums Annaler, 22, 5
Lord, S. D., & Young, J. S. 1990, ApJ, 356, 135
Martínez-García, E. E., & González-López lira, R. A. 2013, ApJ, 765, 105
Martínez-García, E. E., González-López lira, R. A., & Gómez, G. C. 2009, ApJ, 707, 1650
Martínez-García, E. E., & Puerari, I. 2014, ApJ, 790, 118
Michikoshi, S., & Kokubo, E. 2016, arXiv1604.02987
Minchev, I., Famaey, B., Quillen, A. C., Di Matteo, P., Combes, F., Vlajić, M., Erwin, P., & Bland-Hawthorn, J. 2012, A&A, 548, A126
Miyamoto, Y., Nakai, N., & Kuno, N. 2014, PASJ, 66, 36
Navarro, J. F., Frenk, C. S., & White, S. D. M. 1997, ApJ, 490, 493
Oh, S. H., Kim, W.-T., & Lee, H. M. 2015, ApJ, 807, 73
Oh, S. H., Kim, W.-T., Lee, H. M., & Kim, J. 2008, ApJ, 683, 94
Patsis, P. A., Contopoulos, G., & Grosbol, P. 1991, A&A, 243, 373
Pelupessy, F. I., Papadopoulos, P. P., & van der Werf, P. 2006, ApJ, 645, 1024
Pettitt, A. R., Dobbs, C. L., Acreman, D. M., & Bate, M. R. 2015, MNRAS, 449, 3911
Pettitt, A. R., Tasker, E. J., & Wadsley, J. W. 2016, arXiv1603.07801
Pichardo, B., Martos, M., Moreno, E., & Espresate, J. 2003, ApJ, 582, 230
Rix, H.-W., & Zaritsky, D. 1995, ApJ, 447, 82
Roberts, W. W. 1969, ApJ, 158, 123
Roberts, Jr., W. W., & Hausman, M. A. 1984, ApJ, 277, 744
Roca-Fàbrega, S., Valenzuela, O., Figueras, F., Romero-Gómez, M., Velázquez, H., Antoja, T., & Pichardo, B. 2013, MNRAS, 432, 2878
Rots, A. H. 1975, A&A, 45, 43
Rots, A. H., Bosma, A., van der Hulst, J. M., Athanassoula, E., & Crane, P. C. 1990, AJ, 100, 387
Rots, A. H., & Shane, W. W. 1975, A&A, 45, 25
Roškar, R., Debattista, V. P., Quinn, T. R., & Wadsley, J. 2012, MNRAS, 426, 2089
Rydbeck, G., Hjalmarson, A., & Rydbeck, O. E. H. 1985, A&A, 144, 282
Saitoh, T. R., Daisaka, H., Kokubo, E., Makino, J., Okamoto, T., Tomisaka, K., Wada, K., & Yoshida, N. 2008, PASJ, 60, 667
Saitoh, T. R., & Makino, J. 2009, ApJL, 697, L99
—. 2010, PASJ, 62, 301
Salo, H., & Laurikainen, E. 2000a, MNRAS, 319, 377
—. 2000b, MNRAS, 319, 393
Sawa, T. 1977, PASJ, 29, 781
Scarano, S., & Lépine, J. R. D. 2013, MNRAS, 428, 625
Seigar, M. S., & James, P. A. 2002, MNRAS, 337, 1113
Sellwood, J. A. 2011, MNRAS, 410, 1637
Sellwood, J. A., & Binney, J. J. 2002, MNRAS, 336, 785
Sellwood, J. A., & Carlberg, R. G. 1984, ApJ, 282, 61
—. 2014, ApJ, 785, 137
Shetty, R., Vogel, S. N., Ostriker, E. C., & Teuben, P. J. 2007, ApJ, 665, 1138
Shu, F. H., Milione, V., Gebel, W., Yuan, C., Goldsmith, D. W., & Roberts, W. W. 1972, ApJ, 173, 557
Shu, F. H., Milione, V., & Roberts, Jr., W. W. 1973, ApJ, 183, 819
Sundelius, B., Thomasson, M., Valtonen, M. J., & Byrd, G. G. 1987, A&A, 174, 67
Tanikawa, A., Yoshikawa, K., Nitadori, K., & Okamoto, T. 2013, New A., 19, 74
Thomasson, M., & Donner, K. J. 1993, A&A, 272, 153
Thomasson, M., Elmegreen, B. G., Donner, K. J., & Sundelius, B. 1990, ApJL, 356, L9
Toomre, A. 1981, in Structure and Evolution of Normal Galaxies, ed. S. M. Fall & D. Lynden-Bell, 111–136
Tully, R. B. 1974, ApJS, 27, 415
Visser, H. C. D. 1980, A&A, 88, 159
Vogel, S. N., Kulkarni, S. R., & Scoville, N. Z. 1988, Nature, 334, 402
Wada, K. 2008, ApJ, 675, 188

Wada, K., Baba, J., & Saitoh, T. R. 2011, ApJ, 735, 1
Wada, K., & Koda, J. 2004, MNRAS, 349, 270
Wada, K., Papadopoulos, P. P., & Spaans, M. 2009, ApJ, 702, 63
Wolfire, M. G., Hollenbach, D., McKee, C. F., Tielens, A. G. G. M., & Bakes, E. L. O. 1995, ApJ, 443, 152
Woodward, P. R. 1975, ApJ, 195, 61
Zhang, X. 1996, ApJ, 457, 125